Remote Sensing Surface Temperatures of Forests and Melting Snow at Different Spatial Scales

Steven Pestana

A thesis

submitted in partial fulfillment of the

requirements for the degree of

Master of Science in Civil Engineering

University of Washington

2019

Committee:

Jessica Lundquist

David Shean

Program Authorized to Offer Degree:

Civil and Environmental Engineering

University of Washington

Abstract

Remote Sensing Surface Temperatures of Forests and Melting Snow at Different Spatial Scales

Steven Pestana

Chair of the Supervisory Committee

Professor Jessica Lundquist

Civil and Environmental Engineering

Uncooled thermal infrared (TIR) imagers, commonly used on aircraft and small unoccupied aerial systems (UAS, "drones"), can provide high-resolution surface temperature maps, but their accuracy is dependent on reliable calibration sources. A novel method for correcting surface temperature observations made by uncooled TIR imagers uses observations over melting snow, which provides a constant 0 °C reference temperature. This bias correction method is applied to remotely sensed surface temperature observations of forests and snow over two mountain study sites: Laret, Davos, Switzerland (27 March 2017) in the Alps, and Sagehen Creek, California, USA (21 April 2017) in the Sierra Nevada. Surface temperature retrieval errors that arise from temperature-induced instrument bias, differences in image resolution, retrieval of mixed pixels, and variable view angles were evaluated for these forest-snow scenes.

Applying the snow-based bias correction decreased the root-mean-squared error by about 1 °C for retrieving snow, water, and forest canopy temperatures from airborne TIR observations. The degree to which mixed pixels change the observed surface temperature distributions across a forest-snow scene depends not only on image resolution, but also on how the underlying forest is distributed. Airborne observations over forests showed that near the edges of the TIR images, at more than 20° from nadir, the snow surface within forest gaps smaller than 10 m was obscured by the surrounding trees. These off-nadir views could then provide unmixed pixels of canopy surface temperature.

1. Introduction

Thermal infrared (TIR) remote sensing can provide spatially distributed surface temperatures of forests and snow in the mountains where in situ measurements are sparse, and model representation of spatial and temporal heterogeneities is difficult. These measurements of snow surface temperature (T_{ss}) can help evaluate snow surface energy balance model performance (Lapo et al., 2015), while measurements of forest canopy temperature (T_f) provide information about the downward longwave radiation emitted onto the snow below (Webster et al., 2017). Forest canopy temperatures, serving as a proxy for air temperatures (Howard and Stull, 2013), can also provide information about lapse rates and cold air pooling over mountain terrain (Whiteman et al., 2004; Lundquist & Cayan, 2007).

The relatively low cost of both uncooled TIR cameras and small unoccupied aerial systems (UAS) has allowed more researchers to use airborne TIR observations for a variety of applications, including as validation data for testing remote sensing downscaling methods (Lundquist et al., 2018; Wu et al., 2015; Yang et al., 2016). However, methods to constrain the errors associated with airborne TIR instrument bias are needed to improve the accuracy of surface temperature retrievals for these applications. Furthermore, the effects of mixed pixels, where a single pixel covers surfaces of different temperatures, and off-nadir view angles on surface temperature retrievals over forests and snow need better characterization. This is particularly important for airborne observations that are relied on as a source of high spatial resolution ground truth.

This project capitalizes on the uniform temperature of melting snow (0 °C) and uses airborne TIR observations from various altitudes in two forest-snow environments, to answer the following questions:
1. What are the magnitudes of errors in TIR observations of these forest-snow environments caused by instrument bias?
2. Following the snow-based bias correction, how representative of the true surface temperatures are the airborne TIR measurements at different spatial scales?
3. How do image resolution, mixed pixels, and off-nadir view angles contribute to surface temperature retrieval biases over forests and snow?

2. Study Sites, Data, & Instruments

2.1 Study Sites and Observations

A small UAS (Fig. S1c) recorded airborne TIR observations over the Laret, Davos study site (46.845 N, 9.872 E) in eastern Switzerland on 27 March 2017 (13:58 – 14:15 CEST) from altitudes of 40-110 m above ground level (AGL). This site is situated within the sub-alpine forests of the Swiss Alps, about 6 km northeast of the city of Davos (Fig. 1a). At an elevation of 1520 m, this forested site consists largely of Norwegian spruce (*Picea abies*), with some European larch (*Larix decidua*) trees, with heights of 20 - 40 m (Webster et al., 2018). Two meteorological stations provided in situ measurements of T_{SS} from IR radiometers throughout the day, one measuring in an open area, and the other beneath the forest canopy.

On 21 April 2017, a Cessna 172 light aircraft (Fig. S1a) at an altitude of 1000 m AGL (13:16 –13:52 PST) and a small UAS (Fig. S1b) at altitudes of 20-70m AGL (15:15 –15:25 PST) made TIR observations over the Sagehen Creek Field Station (39.432 N, 120.239 W). This site is

within the Tahoe National Forest of the eastern Sierra Nevada in California, USA, about 40 km north of Lake Tahoe and at an elevation of 1950 m (Fig. 1d). The surrounding forest consists largely of lodgepole pines (*Pinus contorta*), with average tree heights of 30 m. In situ measurements of T_{ss} and T_f, were made by a pair of boom-mounted infrared (IR) radiometers (Fig. 1e and S2a) pointed at open snow surface and into a tree canopy, respectively. Hand-held IR radiometer measurements along a series of 20 m transects provided information about the spatial variability of T_{ss} across the study site (Fig. S3). Water temperature (T_w) data for Sagehen Creek from a nearby USGS stream gage (Fig. S2b) was accessed through the USGS National Water Information System (USGS, 2016) (Fig. 1d).
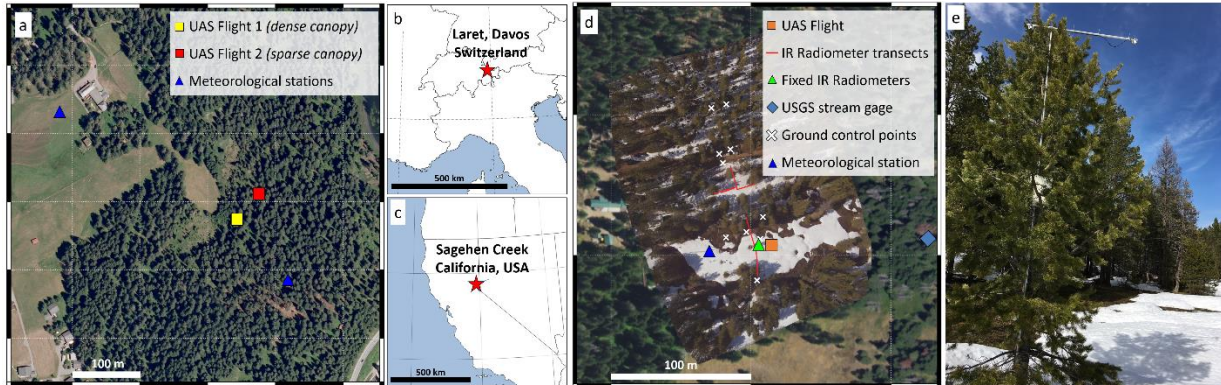

Figure 1. Study sites include (a) Laret, Davos on 27 March 2017 (b) in the Alps of eastern Switzerland, and (c) in the Sierra Nevada of California, USA, (d) Sagehen Creek Field Station on 21 April 2017. (e) IR radiometers measuring the surface temperature of a conifer tree canopy, and the adjacent open snow surface at Sagehen Creek. (Background imagery: a) Copernicus, ESA. 3 October 2009. Davos, Switzerland. 46.85 N, 9.88 E. Google Satellite TMS, and d) National Agriculture Imagery Program, USDA FSA. 12 July 2016. e) Photo by Adrian Harpold.)

2.2 TIR imagers

The TIR imagers used in this study (Table 1; Fig. S1) contain uncooled microbolometer arrays, sensitive to a range of wavelengths in the thermal infrared (Budzier & Gerlach, 2011). Each microbolometer sensor element within the array receives incident radiation within a narrow instantaneous field of view (IFOV). This radiation causes each sensor element to heat up, which changes its electrical resistance, producing a change in voltage that can be measured and recorded. TIR imagers are calibrated to relate these electrical signals to a corresponding spectral radiance – the amount of radiance received within the thermal infrared wavelengths. The temperature of an object within an image scene can then be calculated from this radiance through inverting the Planck equation, which describes the spectral radiance of an object over an interval of wavelengths at a given temperature and emissivity.

The surface temperature measured at each sensor element is a function of all surface temperatures within its IFOV and can be approximated as a linear mixture when all sub-pixel temperatures are within 25 K of each other (McCabe et al., 2008). As image resolution is decreased, a pixel's IFOV is spread across larger areas of a heterogeneous target surface. The ability to measure true surface temperature variability across a heterogeneous surface is reduced at lower resolutions (Liu et al., 2006).

Because these cameras are not actively cooled to maintain a constant temperature, the varying thermal radiation from the camera body itself can result in biases in the retrieved surface temperatures (Shea & Jamieson, 2011). TIR camera body temperatures change due to air temperature, incident sunlight, or self-heating from electrical components. In order to make accurate observations of absolute surface temperatures consistently across a series of images, periodic recalibrations are required to adapt to changing ambient conditions.

Typically, as in the case of the two UAS-mounted TIR cameras, an internal shutter is closed at regular intervals. This provides a reference for the camera body temperature, which is used to update the camera calibration (Ribeiro-Gomes et al., 2017). However, since the shutter is between the lens and microbolometer array, this method does not account for thermal radiation emitted by the externally mounted lens. Alternatively, a second instrument could provide concurrent measurements of surface temperatures to calibrate TIR images in post-processing. This technique was employed with the aircraft's TIR imager, where a nadir-pointing IR radiometer (Fig. S1a) provided independent surface temperature measurements within a narrow field of view. Each image was adjusted so that the mean temperature of the pixels overlapping the 35 m diameter IR radiometer footprint matched the radiometer measurements.

Prior studies using uncooled TIR imagers on UAS have relied on the internal shutters, performed calibrations with blackbody targets prior to or following observations, or used blackbody-like calibration targets with high emissivities, such as water, during the data collection flights (Harvey et al., 2016; Jensen et al., 2014; Webster et al., 2018). Independently measuring the surface temperatures of calibration targets in the field allows for TIR images to be calibrated in post-processing, where images containing the targets can be adjusted to match the independent target temperature measurements, and images without the target in view can be adjusted to match overlapping images that do contain the targets (Gomez-Candon et al., 2016; Sheng et al., 2010). However, setting up calibration targets in the field requires additional resources and can be difficult or impossible in remote or hazardous locations. Repeat imaging of targets by an airborne TIR sensor in a single flight are also needed to provide periodic calibration updates, constraining the spatial extent that can be covered, especially with the short flight times of battery-dependent small UAS. In cases where not every image contains a target, the functional form of the bias, such as linear drift, must be assumed for bias corrections in between calibration images.

	Sagehen Creek Field Station California, USA		Laret, Davos, Switzerland
Aircraft	Cessna 172 *(UW APL)*	Tarot 650 Sport UAS *(AirCTEMPs)*	DJI S1000 UAS *(WSL SLF)*
Flight date and times	4/21/2017 13:16–13:52	4/21/2017 15:15–15:25	3/27/2017 (1) 13:58–14:01, (2) 14:13–14:15
Flight altitudes AGL	1000 m	20 – 70 m	40 – 110 m
TIR Instrument	DRS UC640-17 KT15.85D	ICI 8640P	Optris PI450
Detector size	640 x 480 -	640 x 512	382 x 288
Pixel pitch	17 µm -	17 µm	25 µm
Detector sensitivity (NEΔT)	0.07 °C 0.02 °C	0.02 °C	0.04 °C
Mfr. stated accuracy	- ± 0.5 °C	± 1.0 °C	± 2.0 °C
Spectral range	8 – 14 µm 9.6 – 11.5 µm	7 – 14 µm	7.5 – 13 µm
Focal length	15.5 mm -	12.5 mm	15 mm
Field of view	40° x 30° 1.9°	50° x 37.5°	38° x 29°
Spatial resolution	1.0 - 2.0 m 35 m spot size	0.03 – 0.10 m	0.07 – 0.20 m

Table 1: Aircraft and TIR Instrument Specifications

3. Methods

3.1 TIR Calibration Tests

To quantify and correct for instrument bias in uncooled TIR imagers, we developed and tested a novel bias correction method using the melting snow surface as a natural radiometric calibration target. Ground-based measurements of the snow surface temperature at Sagehen show the snow surface maintaining a constant 0 °C throughout the day (Fig. S3). Snow has a very high emissivity in the thermal infrared, ε≈0.99, independent of snow grain size and largely insensitive to view angles less than 20° (Dozier & Warren, 1982; Warren, 1982), making it very close to an ideal blackbody target. The snow surface temperature measured in each TIR image was determined by finding the coldest peak in the histogram of image pixel values (Fig. 2b). Each TIR image's unique bias was defined as the difference between the temperature at this peak, and the reference melting snow surface temperature of 0 °C. These biases were then subtracted from each image.

To validate the bias corrected ~1.5 m and sub-meter resolution observations, the TIR measured snow, water, and forest canopy temperatures at Sagehen were compared against in situ measurements. Snow surface temperature was retrieved from pixels covering the large snow-covered meadow that was directly measured by the in situ radiometer (aircraft n=84; UAS n=41). Water surface temperatures were retrieved from selected aircraft (n=84) and UAS TIR images (n=25) that presented clear views of the portion of Sagehen Creek in the study area. Four approximately 2.0 m^2 areas along the creek were sampled from both imagery sources, and mean

water surface temperatures were calculated from the pixels within these areas. Forest canopy temperatures were retrieved from a 4.5 m² bounding box (aircraft n=84; UAS n=41) around the small radiometer instrumented tree (Fig. 1e; Fig. 2a).
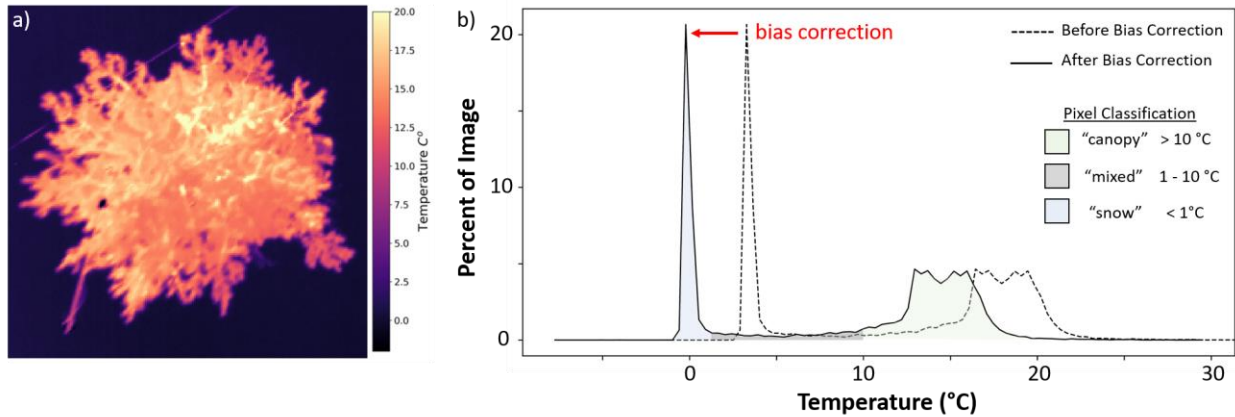

Figure 2. a) TIR image from the UAS over Sagehen, and b) the image histogram before and after bias correction is applied, using the melting snow as a 0 °C temperature reference, with pixels classified by temperature.

3.2 TIR Over Forests and Snow

3.2.1 Image Resolution Tests

The extent to which mixed pixels bias surface temperature retrievals was tested using TIR observations at different image resolutions. Three UAS flights captured TIR imagery over forest canopy areas at a range of image resolutions by gradually raising their altitude while hovering above the canopy crown. This provided image resolutions (ground sample distances) ranging from 3-10 cm for flight altitudes of 20-70 m AGL at Sagehen, and 7-20 cm for flight altitudes of 40-110 m AGL at Davos. Pixels within each area of interest were classified by their temperatures (Fig. 2b) as either unmixed snow pixels (< 1 °C) which were masked out, likely mixed pixels containing both snow and canopy (1-10 °C), or unmixed canopy pixels (> 10 °C).

A linear regression model was fit between image resolution (pixel size in meters), and the fraction of all canopy pixels that were mixed in each image. A second linear regression model was fit between image resolution, and the mean temperature of all non-snow pixels in each image. To determine the significance of these linear regressions, Monte Carlo tests were used to perturb the temperature values of each image by adding a normally distributed error within ±1 °C and re-computing the regressions.

Simulated forest scenes were generated and upscaled (pixel aggregation) to replicate the effect of decreasing resolution. Creating scenes with different forest configurations and fractional vegetated areas (f_{veg}), the proportion of canopy pixels to total pixels as viewed from nadir, allows us to investigate how these factors contribute to the degree of pixel mixing. To represent true surface temperatures of forest canopy and snow surfaces across a 400 m² area at 1 cm resolution, an array of 2000x2000 pixels was created for each simulated scene. Forests were created in two different 2-dimensional configurations (as viewed form nadir) against a snow background: a single circular forest canopy at the center of the scene to represent a dense tree cluster, and a grid of 2 m diameter circular tree canopies spaced at a uniform interval to represent a sparse forest.

All snow pixels were set to 0 °C, and canopy pixels set to 15 °C. Each pair of simulated scenes was created with the same f_{veg}, where the diameter of the cluster in the dense forest, and the spacing between the tree canopies in the sparse configuration were varied to test the impacts at a range of f_{veg} values within 0.1 - 0.8.

To simulate retrieving TIR images of these forest scenes at coarser resolutions, we used a Gaussian kernel to approximate a TIR imager point spread function (PSF) (Cracknell, 1998; Garnier et al., 1999). The PSF encapsulates pixel response to incident radiation given the optical and electrical constraints of the TIR imager, including pixel overlap effects (Calle et al., 2009). Scenes of both forest configurations were then upscaled sequentially from their original 1 cm resolution until the entire simulated scene was contained within one 20 m pixel. A range of f_{veg} values from 0.1 to 0.8 for each forest configuration were tested, and temperature statistics for each upscaled scene were then compared against their original "ground truth" values.

3.2.2 View Angle Tests

We investigated how off-nadir view angles over forests and snow bias surface temperature measurements by looking across the 40°x30° field of view of the aircraft-mounted TIR camera in images of a ~1 km^2 area at Sagehen. This provided us with view angles of up to 35° off-nadir at the image corners. At off-nadir view angles, the use of f_{veg} to describe the linear mixing of forest canopy and snow surface temperatures needs to be substituted for a different measure that takes into account the view geometry over the complex forest canopy surface. Viewable gap fraction (VGF) describes the portion of the ground surface visible between forest canopies at a specific view angle, and has been used in analyses of the view angle effect on visible and shortwave IR observations of fractional snow covered area (Liu et al., 2008; Nolin, 2011; Xin et al., 2012).

Temperature statistics (mean, standard deviation) were computed for each concentric 1° view angle band moving outwards from the image centers at nadir. The fractional area composed of snow pixels (< 1 °C), used as a measure of VGF, was calculated for each 1° field of view band. Linear least-squares regressions were used to fit VGF and the temperature summary statistics with view angle to test for view angle effects on the observed surface temperatures.

To test the ability of these airborne TIR measurements to retrieve snow surface temperature within the viewable gap fraction, small forest gaps were identified around the Sagehen site with diameters ranging from 10 m to 2 m. Pixel temperatures form the aircraft's 1.5 m resolution TIR imagery were retrieved from the center 3x3 pixels within each of these gaps to compare against in situ snow surface temperature.

4. Results

4.1 TIR Calibration Results

The use of melting snow surface temperature ($T_{ss} = 0$ °C) as a calibration reference for instrument bias correction (Section 3.1) was validated against in situ measurements of snow, water, and tree canopy temperatures at Sagehen. These results are summarized as root-mean-squared errors before and after bias correction in Table 2.

TIR System and Resolution		RMSE Before (°C)	RMSE After (°C)
Aircraft: ~1.5 m, TIR camera + radiometer	T_{ss}	1.5	0.2
	T_w	2.4	1.7
	T_f	*N/A*	*N/A*
UAS: ~0.1 m, TIR camera	T_{ss}	2.0	0.7
	T_w	2.1	1.0
	T_f	3.3	2.3

Table 2: Root-mean-squared errors of airborne TIR measurements at Sagehen Creek before and after bias correction for snow (T_{ss}), water (T_w), and forest canopy (T_f) surface temperatures.

The UAS TIR system had a larger range of surface temperature retrieval biases (-2.9 – 3.0 °C), than the aircraft system (0.7 – 2.2 °C), and higher baseline RMSE over snow (Table 2). The difference in bias magnitudes seen between the two systems is likely due to the aircraft's concurrent radiometer measurements used for onboard correction. This provided a constant update for the TIR camera calibration, rather than the periodic calibrations with the internal shutters used on the UAS TIR system. However, the aircraft was unable to resolve the temperature of the small instrumented tree canopy (Fig. 1e). Issues related to image resolution are discussed further in Section 4.2. The bias correction using melting snow surfaces as a reference decreased RMSE by about 1.0 °C in all other cases (Table 2).

There were no identifiable patterns in bias over time since the shutter closed in the UAS system, suggesting that biases are not a function of linear drift, but instead are controlled by external factors that affect the TIR camera body temperature, such as ambient air temperature or incident sunlight on the camera body. Our results also suggest that periodic calibrations (i.e. internal shutter) are not as effective as having a reference temperature present in each scene.

4.2 TIR Over Forests and Snow Results

4.2.1 Effects of Image Resolution and Forest Structure

We tested the effects of image resolution and forest structure (sparse vs. clumped) on the sensor's ability to retrieve actual T_{ss} and T_f using our three field sites and simulated data (Fig. 3). At Sagehen's single tree surrounded by open snow (Fig. 1e & 3a), the fraction of canopy contained within mixed pixels increased by 20% as image resolutions decreased from 3 to 10 cm (Fig. S4a). As the pixels containing canopy mixed more with the adjacent snow surfaces with decreasing resolutions, the mean retrieved T_f decreased by more than 3 °C (Fig. S4b). For the two tree clusters at Davos, where image resolutions decreased from 7 to 20 cm, there were less significant changes in mixed pixel fractions and mean retrieved T_f. The mixed pixel fraction increased by less than 5%, and there was no statistically significant change in retrieved mean T_f

at the tree cluster in the more densely forested area (Fig. 3b). The tree cluster surrounded by open snow (Fig. 3c) saw an increase of mixed pixels by 10% and decrease in mean retrieved T_f of 2 °C.

Mixed pixels dominated the simulated sparse forest scenes when f_{veg} was < 0.7. With these low f_{veg} values, individual 2 m diameter tree canopies could not be resolved without pixels mixing with the surrounding snow surface. Only at f_{veg} > 0.7 when the small tree canopies were close enough together could the simulated observations retrieve unmixed canopy temperatures. Conversely, unmixed snow surface temperatures could only be retrieved with f_{veg} < 0.25 with this sparse forest configuration. As an illustrative example (Fig. 3d), the simulated sparse forest scene with f_{veg} = 0.13 shows all of the trees contained within mixed pixels whereas the snow surface is not, when observed at a resolution of ~1.5 m. This figure resembles the aircraft TIR observations of the isolated tree canopy at Sagehen (Fig. 3a), which resulted in a large T_f RMSE (11.7 °C) as the canopy blurred with the surrounding snow surface. The retrieved surface temperature distribution over a sparse forest with significant pixel mixing will not reflect the true surface temperature variability (Fig. S5a). In contrast to sparse forests, the simulated observations of a dense tree cluster could retrieve T_f from unmixed pixels at a wide range of f_{veg} values. Also illustrated with an f_{veg} = 0.13 in Figure 3e, this dense forest cluster had only 42% of its canopy contained within mixed pixels at ~1.5 m resolution, and the true canopy temperature could be retrieved from pixels at the center of the cluster, away from its edges. Observations of a forest structured with dense tree clusters like this would retrieve a surface temperature distribution closer to that of the true variability (Fig. S5b), which could be used to identify the two end-members (trees and snow) as the warmest and coldest points, respectively, within the scene.
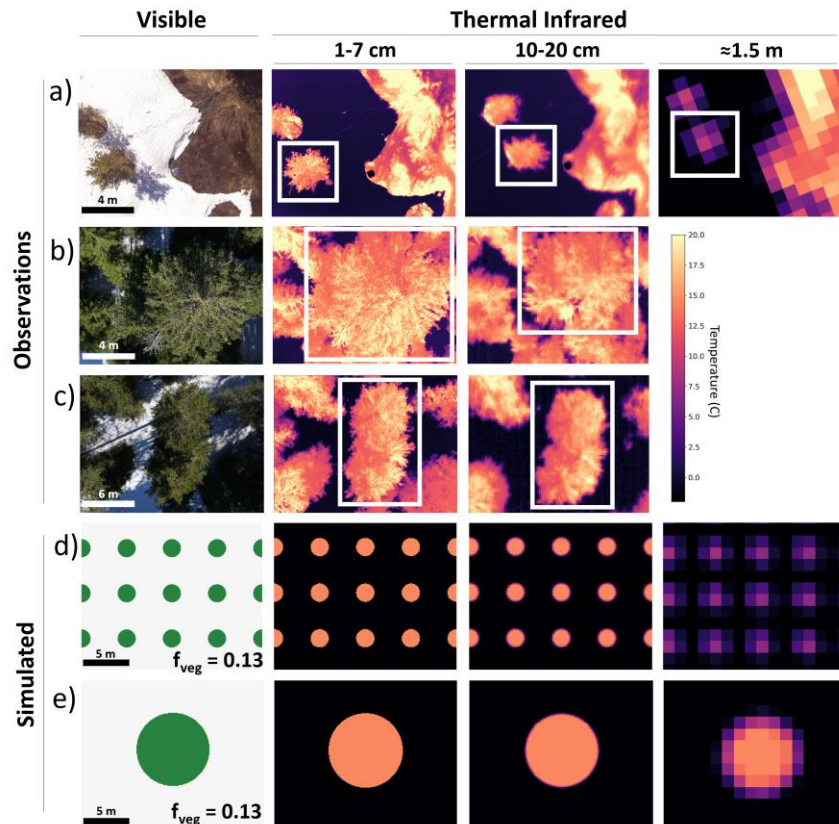

Figure 3. Observing forest canopy temperatures against snow surfaces at a range of image resolutions. a) A single small tree canopy at Sagehen, b) a tree cluster in a densely forested area at Davos, c) a tree cluster in a more sparsely forested area at Davos, d) simulated sparse forests, and e) simulated dense tree cluster.

4.2.2 Effects of Off Nadir View Angles

As off-nadir view angles increased (Fig. 4a), the mean VGF at Sagehen decreased at a rate of 0.9% per degree (from over 30% at nadir to less than 5% at 35° off-nadir) (Fig. S6a). The mean pixel temperature increased with increasing off-nadir view angles, at a rate of 0.05 °C per degree (Fig. S6b). This translated to higher apparent temperatures (+1.75°C) at image edges than the center, as snow in forest gaps was obscured by the warmer forest canopy. The standard deviation of measured surface temperatures decreased by 1.1 °C as view angles increased and mean temperatures converged towards canopy temperatures (Fig. S6c). With TIR observations at 1.5 m resolution, the snow surface temperatures retrieved from within visible forest gaps were most accurate for gaps larger than 10 m in diameter. With decreasing gap sizes (Fig. 4b), TIR observations of the snow surface temperatures within them became biased higher as more of the retrieved pixels were mixed, approaching the temperature of the surrounding forest canopy.
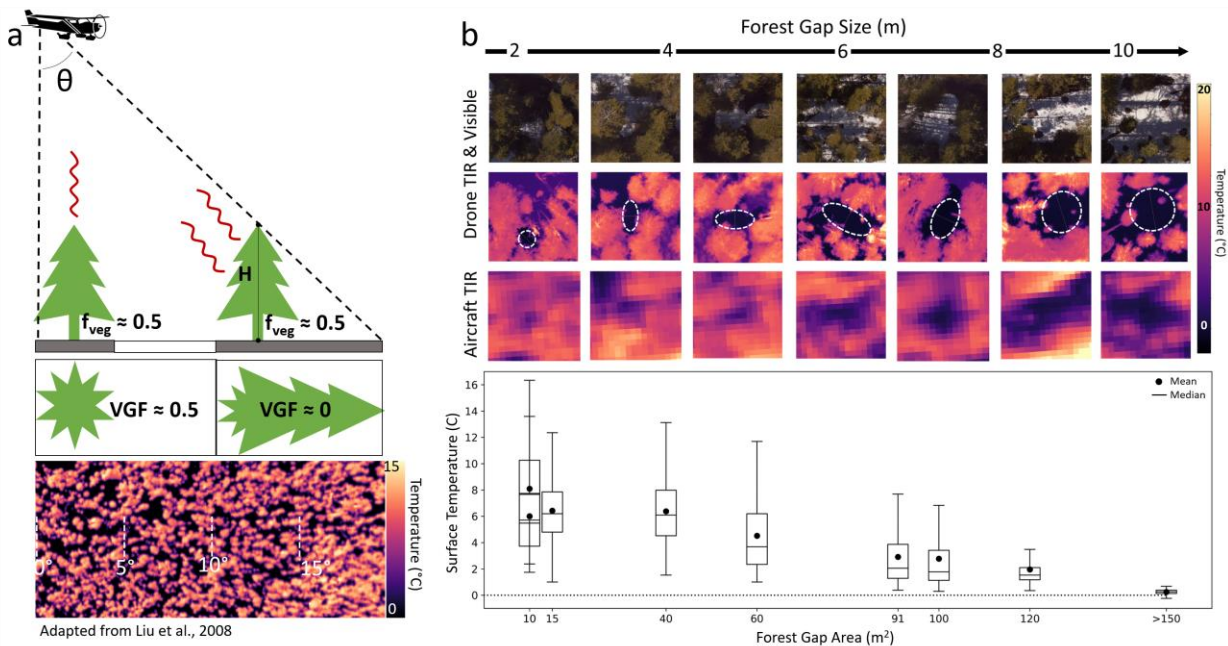

Figure 4. a) Demonstration of the effects of off-nadir view angle over forests and snow, where forest gaps are obscured by trees near the edges of the image field of view. b) Retrieving snow surface temperature from small forest gaps shows substantial pixel mixing with the surrounding forest canopy for gaps smaller than about 5 pixels wide.

5. Discussion and Applications

5.1 Melting Snow as a TIR Calibration Target

Using melting snow as a constant 0 °C reference for bias correction decreased surface temperature retrieval errors for uncooled TIR imagers. For features that could be resolved by the sub-meter resolution UAS TIR and ~1.5 m resolution aircraft TIR, surface temperature RMSE's were reduced by about 1 °C using this method. Correcting for this instrument bias is needed for airborne observations, where ambient air temperature and incident sunlight that change the

camera body temperature are not compensated for quickly enough by the internal shutter recalibrations. This is essential when observations of absolute surface temperatures or inter-image comparisons of surface temperatures are needed, rather than relative temperature differences within a single image.

Without melting snow surfaces at a study site, airborne TIR observations over a small area could instead rely on targets maintained within the TIR camera's field of view, so that a unique bias correction could be determined and applied to each image. However, for the more common scenario of airborne TIR observations over large areas, installing multiple targets is logistically difficult. Instead, including a second, higher accuracy IR radiometer sampling alongside the TIR camera could provide a better source for bias corrections, rather than having to rely on the intermittent re-calibrations using an internal shutter common on many of these TIR cameras. Though the additional instrumentation mass could preclude small UAS from doing this, limiting the method to only larger airborne platforms.

5.2 TIR Image Resolution and View Angles Over Snow and Forests

Airborne TIR observations at a range of spatial resolutions demonstrated the linear mixing of subpixel forest and snow temperatures (McCabe et al., 2008), where at lower resolutions the mean retrieved canopy temperatures at forest edges were biased lower as they became blurred with the adjacent snow surfaces. Retrieving accurate, unmixed, surface temperatures of small features, such as narrow streams like Sagehen Creek, requires an image resolution high enough to cover the feature with at least 3 pixels (Handcock et al., 2006). This was seen in our attempts to retrieve the canopy temperature of a single small tree (Fig. 3a), and snow surface temperature within forest gaps smaller than 10 m (Fig. 4b). This pixel mixing occurs within the forest canopy as well, between warmer sunlit and cooler shaded branches blurring towards a mean canopy temperature (Fig. S7).

The simulated forest scenes showed that TIR remote sensing retrieves different surface temperature distributions over forest-snow environments depending on the forest structure, and not on f_{veg} alone. Sparsely forested areas have more forest edges susceptible to blurring with adjacent snow, and with more mixed pixels, their temperature distributions will be biased towards a mean of the two temperature end-members. Observations over forests with large tree clumps and/or wide forest gaps will have fewer mixed pixels, and could retrieve temperature distributions that better represent the true distribution.

When observed from off-nadir view angles, the forest's VGF decreased and mean retrieved temperatures increased as trees obscured more of the snow surface behind and beneath them. While off-nadir view angles may hinder measurements of snow surface temperature within forests, they present an opportunity to retrieve unmixed canopy temperature pixels even with coarser resolution observations. Observations of forests at large view angles would allow measurements of canopy temperature regardless of ground cover, and could be applied to studying seasonal mountain meteorological conditions (Essery et al., 2008), informing models of longwave radiation over snowpack (Webster et al., 2017), or monitoring forest health (Wang & Dickinson, 2012). However, observations from these view angles would also need to consider the direction of incident sunlight (Henderson et al., 2003) to determine if observations are biased due to viewing sunlit or shaded portions of the canopy (Fig. S8).

5.3 Implications for Satellite Remote Sensing of Forests and Snow

For satellite thermal infrared remote sensing over heterogeneous forest-snow areas, with pixel resolution of ~1-2 km (VIIRS, MODIS, GOES ABI), we could expect to retrieve a mean, linearly mixed surface temperature in proportion to the pixel's f_{veg} at nadir, or to the VGF when off-nadir. Satellite observations of the same area at higher resolutions of 70-100 m (ECOSTRESS, ASTER, Landsat 8 TIRS), could only reliably provide unmixed pixels of the two temperature end-members where continuous canopy or open snow cover areas are larger than 300x300 m.

A parameter to quantify forest structure, such as a canopy gap size distribution (Mazzotti et al., in review), could be used to describe the degree of bias in the observed surface temperature distribution we could expect to have due to mixed pixels. Spectral unmixing methods used to retrieve forest and snow temperatures from these mixed pixels need the local VGF determined for off-nadir view angles. This VGF can be calculated through models that use independent forest structure information (Liu et al., 2008), or by solving directly for the fractional viewable snow covered area (equal to 1-VGF) across multiple adjacent pixels at once (Lundquist et al., 2018).

6. Conclusion

Instrument bias of uncooled TIR cameras was identified as a significant source of error, impacting the measurement of accurate surface temperatures from airborne platforms. We applied a bias correction method using the constant 0 °C melting snow surface as a natural calibration target, and demonstrated its ability to improve the accuracy of airborne TIR surface temperature measurements. The observed temperature distribution of a forest-snow scene was found to depend on image resolution and the underlying forest structure. Coarse resolution observations of sparse forests with more edges will retrieve more mixed pixels than the observations of a forest with dense tree clumps and large gaps at the same resolution. At off-nadir view angles greater than 20°, the forest canopy began to obscure snow in forest gaps from view, biasing the mean temperatures retrieved from image edges higher than those from image centers, though these off-nadir views could allow canopy temperature measurements without the issue of including mixed pixels from the snow or ground surface below.

References:

Budzier, H., & Gerlach, G. (2011). *Thermal Infrared Sensors. Proceedings of the National Academy of Sciences of the United States of America* (Vol. 104). Chichester, UK: John Wiley & Sons, Ltd. https://doi.org/10.1002/9780470976913

Calle, A., Casanova, J. L., & González-Alonso, F. (2009). Impact of point spread function of MSG-SEVIRI on active fire detection. *International Journal of Remote Sensing*, *30*(17), 4567–4579. https://doi.org/10.1080/01431160802609726

Cracknell, A. P. (1998). Review article Synergy in remote sensing-what's in a pixel? *International Journal of Remote Sensing*, *19*(11), 2025–2047. https://doi.org/10.1080/014311698214848

Dozier, J., & Warren, S. G. (1982). Effect of viewing angle on the infrared brightness temperature of snow. *Water Resources Research*, *18*(5), 1424–1434. https://doi.org/10.1029/WR018i005p01424

Essery, R., Bunting, P., Rowlands, A., Rutter, N., Hardy, J., Melloh, R., … Pomeroy, J. (2008). Radiative Transfer Modeling of a Coniferous Canopy Characterized by Airborne Remote Sensing. *Journal of Hydrometeorology*, *9*(2), 228–241. https://doi.org/10.1175/2007JHM870.1

Mouclier, C., Garnier, C., Rousee, F., Collorec, R., & Flifla, J. (2008). Infrared sensor modeling for realistic thermal image synthesis (pp. 3513–3516 vol.6). https://doi.org/10.1109/icassp.1999.757600

Gómez-Candón, D., Virlet, N., Labbé, S., Jolivot, A., & Regnard, J. L. (2016). Field phenotyping of water stress at tree scale by UAV-sensed imagery: new insights for thermal acquisition and calibration. *Precision Agriculture*, *17*(6), 786–800. https://doi.org/10.1007/s11119-016-9449-6

Handcock, R. N., Gillespie, A. R., Cherkauer, K. A., Kay, J. E., Burges, S. J., & Kampf, S. K. (2006). Accuracy and uncertainty of thermal-infrared remote sensing of stream temperatures at multiple spatial scales. *Remote Sensing of Environment*, *100*(4), 427–440. https://doi.org/10.1016/j.rse.2005.07.007

Harvey, M. C., Rowland, J. V., & Luketina, K. M. (2016). Drone with thermal infrared camera provides high resolution georeferenced imagery of the Waikite geothermal area, New Zealand. *Journal of Volcanology and Geothermal Research*, *325*(June), 61–69. https://doi.org/10.1016/j.jvolgeores.2016.06.014

Henderson, B. G., Balick, L. K., Rodger, A. P., & Pope, P. A. (2004). Concurrent measurements of directional reflectance and temperature of a wintertime coniferous forest from space. *Ecosystems' Dynamics, Agricultural Remote Sensing and Modeling, and Site-Specific Agriculture*, *5153*(December 2003), 21. https://doi.org/10.1117/12.506296

Howard, R., & Stull, R. (2013). IR radiation from trees to a ski run: A case study. *Journal of Applied Meteorology and Climatology*, *52*(7), 1525–1539. https://doi.org/10.1175/JAMC-D-12-0222.1

Jensen, A. M., McKee, M., & YangQuan Chen. (2014). Procedures for processing thermal images using low-cost microbolometer cameras for small unmanned aerial systems. *2014 IEEE Geoscience and Remote Sensing Symposium*, 2629–2632. https://doi.org/10.1109/IGARSS.2014.6947013

Lapo, K. E., Hinkelman, L. M., Raleigh, M. S., & Lundquist, J. D. (2015). Impact of errors in the downwelling irradiances on simulations of snow water equivalent, snow surface temperature, and the snow energy balance. *Water Resources Research*, *51*(3), 1649–1670. https://doi.org/10.1002/2014WR016259

Liu, Y., Hiyama, T., & Yamaguchi, Y. (2006). Scaling of land surface temperature using satellite data: A case examination on ASTER and MODIS products over a heterogeneous terrain area. *Remote Sensing of Environment*, *105*(2), 115–128. https://doi.org/10.1016/j.rse.2006.06.012

Liu, H., & Weng, Q. (2008). Seasonal variations in the relationship between landscape pattern and land surface temperature in Indianapolis, USA. *Environmental Monitoring and Assessment*, *144*(1–3), 199–219. https://doi.org/10.1007/s10661-007-9979-5

Lundquist, J. D., & Cayan, D. R. (2007). Surface temperature patterns in complex terrain: Daily variations and long-term change in the central Sierra Nevada, California. *Journal of Geophysical Research Atmospheres*, *112*(11). https://doi.org/10.1029/2006JD007561

Lundquist, J. D., Chickadel, C., Cristea, N., Currier, W. R., Henn, B., Keenan, E., & Dozier, J. (2018). Separating snow and forest temperatures with thermal infrared remote sensing. *Remote Sensing of Environment*, *209*(September 2017), 764–779. https://doi.org/10.1016/j.rse.2018.03.001

Mazzotti, G., Currier, W.R., Deems, J.S., Pflug, J.M., Lundquist, J.D., Jonas, T. (2019). Revisiting Snow Cover Variability and Canopy Structure within Forest Stands: Insights from Airborne Lidar Data. Manuscript submitted for publication.

McCabe, M. F., Balick, L. K., Theiler, J., Gillespie, A. R., & Mushkin, A. (2008). Linear mixing in thermal infrared temperature retrieval. *International Journal of Remote Sensing*, *29*(17–18), 5047–5061. https://doi.org/10.1080/01431160802036474

Nolin, A. W. (2011). Recent advances in remote sensing of seasonal snow. *Journal of Glaciology*, *56*(200), 1141–1150. https://doi.org/10.3189/002214311796406077

Rademacher, L. K., Clark, J. F., Clow, D. W., & Hudson, G. B. (2005). Old groundwater influence on stream hydrochemistry and catchment response times in a small Sierra Nevada catchment: Sagehen Creek, California. *Water Resources Research*, *41*(2), 1–10. https://doi.org/10.1029/2003WR002805

Ribeiro-Gomes, K., Hernández-López, D., Ortega, J. F., Ballesteros, R., Poblete, T., & Moreno, M. A. (2017). Uncooled thermal camera calibration and optimization of the photogrammetry process for UAV applications in agriculture. *Sensors (Switzerland)*, *17*(10), 9–11. https://doi.org/10.3390/s17102173

Shea, C., & Jamieson, B. (2011). Some fundamentals of handheld snow surface thermography. *Cryosphere*, *5*(1), 55–66. https://doi.org/10.5194/tc-5-55-2011

Sheng, H., Chao, H., Coopmans, C., Han, J., McKee, M., & Chen, Y. Q. (2010). Low-cost UAV-based thermal infrared remote sensing: Platform, calibration and applications. *Proceedings of 2010 IEEE/ASME International Conference on Mechatronic and Embedded Systems and Applications, MESA 2010*, 38–43. https://doi.org/10.1109/MESA.2010.5552031

U.S. Geological Survey (USGS), 2016, National Water Information System data available on the World Wide Web (USGS Water Data for the Nation), accessed August 2018, at URL https://waterdata.usgs.gov/nwis/inventory?agency_code=USGS&site_no=10343500 http://dx.doi.org/10.5066/F7P55KJN

Wang, K., & Dickinson, R. E. (2012). A review of global terrestrial evapotranspiration: observation, modelling, climatology, and climatic variability. *Review of Geophysics*, *50*(2011), 1–54. https://doi.org/10.1029/2011RG000373.1.INTRODUCTION

Warren, S. G. (1982). Optical properties of snow. *Reviews of Geophysics*. https://doi.org/10.1029/RG020i001p00067

Webster, C., Rutter, N., & Jonas, T. (2017). Improving representation of canopy temperatures for modeling subcanopy incoming longwave radiation to the snow surface. *Journal of Geophysical Research: Atmospheres*, *122*(17), 9154–9172. https://doi.org/10.1002/2017JD026581

Webster, C., Westoby, M., Rutter, N., & Jonas, T. (2018). Three-dimensional thermal characterization of forest canopies using UAV photogrammetry. *Remote Sensing of Environment*, *209*(March 2017), 835–847. https://doi.org/10.1016/j.rse.2017.09.033

Whiteman, C. D. (2004). Comparison of Vertical Soundings and Sidewall Air Temperature Measurements in a Small Alpine Basin. *Journal of Applied Meteorology*, *43*(11), 1635–1647.

Wu, P., Shen, H., Zhang, L., & Göttsche, F. M. (2015). Integrated fusion of multi-scale polar-orbiting and geostationary satellite observations for the mapping of high spatial and temporal resolution land surface temperature. *Remote Sensing of Environment*, *156*, 169–181. https://doi.org/10.1016/j.rse.2014.09.013

Xin, Q., Woodcock, C. E., Liu, J., Tan, B., Melloh, R. A., & Davis, R. E. (2012). View angle effects on MODIS snow mapping in forests. *Remote Sensing of Environment*, *118*(10), 50–59. https://doi.org/10.1016/j.rse.2011.10.029

Yang, G., Weng, Q., Pu, R., Gao, F., Sun, C., Li, H., & Zhao, C. (2016). Evaluation of ASTER-like daily land surface temperature by fusing ASTER and MODIS data during the HiWATER-MUSOEXE. *Remote Sensing*. https://doi.org/10.3390/rs8010075